

Dynamics of negative muonium in *n*-type silicon

B. Hitti and S. R. Kreitzman

TRIUMF, 4004 Wesbrook Mall, Vancouver, British Columbia, Canada V6T 2A3

T. L. Estle

Department of Physics, Rice University, Houston, Texas 77251-1892

E. S. Bates, M. R. Dawdy, T. L. Head, and R. L. Lichti

Department of Physics, Texas Tech University, Lubbock, Texas 79409-1051

(Received 26 June 1998)

Temperature-dependent diamagnetic amplitudes from radio-frequency muon spin-resonance data on two moderately to heavily doped *n*-type silicon samples require the presence of Mu_T^- . We determine the Mu_T^- to Mu_T^0 ionization energy to be 0.56 ± 0.03 eV for silicon, considerably higher than the Mu_{BC}^0 to Mu_{BC}^+ ionization energy of 0.21 ± 0.01 eV. Thus muonium will be a negative- U impurity only if the energy difference between the Mu_T^- and Mu_{BC}^0 configurations is less than 0.35 eV. The $\text{Mu}(0/+)$ thermodynamic level correlates well with results for monatomic hydrogen, but the $\text{Mu}(-/0)$ level is estimated to be shallower than that claimed for $\text{H}(-/0)$. The muonium data show a complicated set of transitions active during the muon lifetime, and involving four separate muonium states. Similar rapid transitions should be considered when interpreting data on isolated hydrogen centers. [S0163-1829(99)11107-X]

I. INTRODUCTION

The structure and dynamics of muonium ($\text{Mu} = \mu^+ e^-$) in crystalline silicon have long been recognized as directly relevant to understanding the analogous hydrogen defect centers in semiconductors.¹⁻⁴ Hydrogen impurities are of interest primarily because of their ability to electrically passivate many impurities and defects. Isolated hydrogen is difficult to study, since high concentrations of a single state are required, and H quickly forms complexes with itself or other defect species. In comparison, muonium nearly always remains isolated for times on the order of the muon lifetime ($\tau_\mu \approx 2.2 \mu\text{s}$). The muon has a mass m_μ approximately $\frac{1}{9}$ th that of the proton m_p , and Mu can be considered a light isotope of hydrogen with qualitatively similar chemical and physical properties.

Two types of neutral interstitial muonium centers have been observed at low temperature in semiconductors. The stable configuration of Mu^0 in Si has the muon at or near a bond-center (BC) site Mu_{BC}^0 ; the second configuration is metastable in Si and is located within a tetrahedral (T) interstitial region Mu_T^0 . In addition to these neutral states, charged muonium centers occur. In *p*-type Si, the charged center is positive and channeling studies⁵ have shown it to reside near a BC site Mu_{BC}^+ , consistent with theoretical expectations.^{1,2} In this paper we report on results for the negative charge state which we observe in moderately to heavily doped *n*-type Si, and which is stable² in the tetrahedral configuration Mu_T^- .

Of particular interest are the dynamics of transitions among the four states of muonium. Earlier we reported detailed measurements⁶ on transitions involving Mu_{BC}^0 , Mu_T^0 , and Mu_{BC}^+ , which are the only states present appreciably in *p*-type, intrinsic, and low-concentration *n*-type Si, and qualitatively described the behavior of Mu^- required to explain

several features in *n*-type samples at intermediate doping levels. Delayed formation of the negative charge state from the Mu_{BC}^0 initial fraction compared to the rate originating from Mu_T^0 , as previously reported,^{6,7} confirms that a site change is required consistent with the expected Mu_T^- configuration. In the present paper we present more detailed results for transitions involving neutral muonium and Mu_T^- which dominate in more heavily doped *n*-type Si. Our analysis indicates that Mu_T^- thermally ionizes with an ionization energy of 0.56 eV, leaving Mu in the metastable neutral state Mu_T^0 . This result establishes that the T -site negative \rightarrow neutral ionization energy for muonium is greater than the neutral \rightarrow positive ionization energy for the BC site which was previously determined to be 0.21 eV.⁶ The BC result closely corresponds to the thermodynamic $\text{Mu}(0/+)$ level depth, while the T -site ionization measurement represents an extreme upper limit on the depth of $\text{Mu}(-/0)$ below the conduction-band edge, as discussed below. We must stress that within the muon lifetime the muonium defect system does not reach thermal equilibrium, except perhaps at very high temperatures. Therefore, unlike typical measurements on hydrogen impurities, observed transitions are those which drive the system toward equilibrium, rather than those which would eventually maintain the mix of populations under (dynamic) equilibrium conditions.

Fast capacitance transient measurements⁸ have placed the thermodynamic acceptor level for monatomic hydrogen near midgap in crystalline Si, more than 0.3 eV below the donor level, leading to the conclusion that hydrogen has a large negative "effective Coulomb energy"; *i.e.*, that hydrogen is a negative- U impurity. In such a system two neutral hydrogen defect centers can lower their energy by changing to H^+ and H^- as (quasistatic) equilibrium states. In comparing hydrogen and muonium energy relationships, one must account for the fact that the Mu energy level results are based on

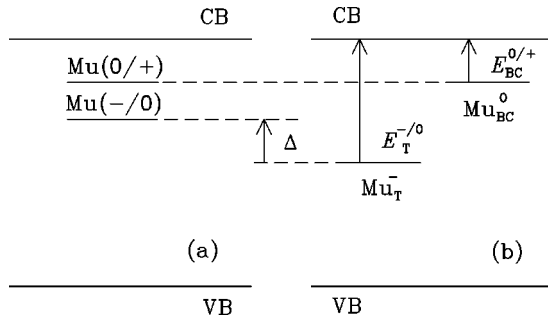


FIG. 1. The relationship between thermodynamic levels (a) and the single-site electronic energies (b) for muonium in silicon. The configurational contribution Δ is significant, but not known experimentally. The very small differences in the configuration energy for different charge states at each individual site are neglected.

ionization dynamics and represent energy differences between two charge states *at a single site*, while the hydrogen numbers are assigned to energy differences between the *stable configurations* for each charge state, H_{BC}^+ , H_{BC}^0 , and H_T^- . The essential difference is that the change in the configurational energy between the metastable state Mu_T^0 and ground state $\text{Mu}_{\text{BC}}^0(\Delta)$ must be included in the Mu acceptor level in addition to the *T*-site “ionization” energy, giving $\text{Mu}(-/0) = E_T^{-/0} - \Delta$. Figure 1 explicitly shows the relationships we are assuming between the single-site electronic energies for muonium and the associated thermodynamic levels as traditionally used in discussing impurity states in semiconductors.⁹ In constructing this diagram we have also assumed that the Mu ionization processes place the ionized e^- at the bottom of the conduction band.

A second important result from investigations of muonium dynamics is that our data show quite rapid charge-state conversions involving all four of the Mu states which are much more complicated than the reactions assumed in analyzing the hydrogen data,⁸ thus raising some questions regarding the validity of the assumptions underlying that analysis. A critical assumption, based in part on details of the calculational model,⁸ was that no metastable H^0 state exists in silicon. For the analogous muonium system the metastable Mu_T^0 is separated from the ground state Mu_{BC}^0 by a barrier of 0.38 eV. If one accepts that the physical properties of Mu and H centers are qualitatively similar at ordinary temperatures, then equivalent transitions involving a metastable H_T^0 state should be included in the analysis of data on hydrogen dynamics.

II. EXPERIMENTAL DETAILS

The technique used in this study, referred to as radio-frequency muon spin resonance (rf- μ SR), has been described in detail elsewhere.⁶ Two features of this method make it particularly attractive for the present study. (1) The experiment, performed in a longitudinal field (lf) geometry, detects a given center independently of whether it is formed promptly upon muon implantation or formed slowly by a transition from a precursor Mu state. This is not generally the case in transverse field (tf), experiments where the requirement of phase coherence limits observation of final states to only those transitions occurring within a small fraction of the

precession period for the muon spin in the precursor state. (2) The presence of a strong rf field implies that only a center which satisfies the resonance condition is detected. These features make the rf technique ideally suited for investigating transitions among the various muonium centers in semiconductors.

The most recent experiments were performed at TRI-University Meson Facility, where positive muons with $\approx 100\%$ spin polarization were implanted into two silicon samples, designated as *N15* and *N16*. *N15* has a net phosphorus (P) concentration of $1.5 \times 10^{15} \text{ cm}^{-3}$ and a $\langle 100 \rangle$ face, and *N16* is a $\langle 111 \rangle$ sample with a donor concentration of $5 \times 10^{15} \text{ cm}^{-3}$. The amplitude of the diamagnetic signal was measured at a fixed oscillator frequency of 27.1 MHz by varying the external magnetic field around 2 kG. The field was applied parallel to the $\langle 100 \rangle$ and $\langle 111 \rangle$ crystallographic direction for *N15* and *N16*, respectively. Both of these samples were used in the previous study.⁶ In that experiment⁶ a thermocouple, placed outside the coil on the boron nitride substrate used to mount the sample, measured the temperature difference between the substrate and a calibrated Si diode located on the Cu housing that holds the coil assembly. Because of the heavy doping the rf heating of the *N16* sample itself due to eddy currents was large, resulting in a large temperature gradient and a large uncertainty in the temperature of the sample. To determine the temperature more accurately, we re-examined both *N15* and *N16* at reduced rf power to minimize the heating and with a platinum thermometer placed inside the rf coil in much better thermal contact with the sample. For the new measurement an rf power of 100 W was used to produce a B_1 of about 5 G inside the coil. Under these conditions the uncertainty in the measured temperature was less than 1 K. The improved temperature measurement has allowed us to reliably distinguish dynamic features related to transitions involving Mu^- , and to determine more accurately the relevant dynamic parameters.

III. DYNAMIC MODEL AND ANALYSIS METHODS

Observed transitions among the Mu states in Si are represented schematically in Fig. 2. The solid arrows represent the transitions active in near intrinsic and *p*-type samples, and the dashed arrows additional interactions which become important in *n*-type samples. Because of the increased concentration of conduction electrons, e^- scattering and capture processes are much more important in *n*-type samples than in *p*-type and near-intrinsic samples. When the rate for electron capture by Mu_T^0 is fast compared to the inverse muon lifetime, Mu_T^- will form at lower temperatures, where the $\text{Mu}_T^0 \rightarrow \text{Mu}_{\text{BC}}^0$ site change remains slow. Additionally, conduction electron scattering which can flip the Mu^0 electron’s spin becomes an important depolarizing mechanism, and other e^- capture transitions are enhanced. One of these, e^- capture at Mu_{BC}^0 , will also lead to a Mu_T^- final state. Thus at higher temperatures, transitions out of Mu_T^- can be investigated provided that the formation probability for this state remains sufficiently high.

The model we have used in an updated fit to the rf- μ SR data is a more complete version of the strong collision model used previously.⁶ A full set of parameters resulting from the more complete model are given in Table I. In addition to

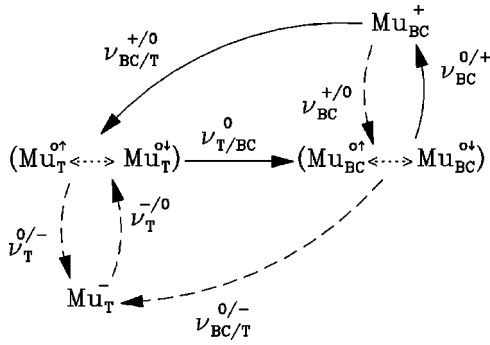


FIG. 2. Observed transitions among the four muonium states in silicon. The solid lines are for reactions active in p -type samples and at high temperature in the lightly doped n -type samples. The broken lines are for processes important in moderately to heavily doped n -type samples and in the lightly doped samples at low temperature. Different e^- spin orientations within the two Mu^0 states are indicated separately.

including a fourth state, Mu_T^- , and the associated transitions, the new version more accurately models the muon polarization following recapture of an e^- by Mu_{BC}^+ by separately treating electrons having the same and opposite spin orientation as the preionization electron; see the Appendix. Since the hyperfine parameter of Mu_{BC}^0 is anisotropic, the effective magnetic field at the muon due to the unpaired electron differs depending on the direction of the electron spin. As a result, when Mu_{BC}^0 ionizes, the polarization transferred to the ionized product has a complicated temperature dependence which was treated in Appendix B of Ref. 6. Qualitatively, the anisotropy of Mu_{BC}^0 produces a double step in the diamagnetic amplitude vs temperature curve resulting from the ionization. However, when electrons are recaptured by Mu_{BC}^+ , the result is a charge-exchange cycle and the differences due to the e^- spin orientation become effectively averaged. The net effect is that when the recapture rate becomes sufficiently rapid a single step at a some-

what higher temperature replaces the double step in the diamagnetic amplitude.¹⁰ In addition, charge exchange and a similar spin-exchange process due to spin-flip scattering are very effective muon depolarizing mechanisms when the exchange rates are approximately equal to the Mu^0 hyperfine frequency. Proper modeling of the Mu_{BC} charge cycles and related depolarization mechanisms is especially important for weakly n -type samples, and yields significantly improved parameters for e^- capture.¹⁰

Temperature-dependent ionization, activation, and capture rates are used to describe the dynamics of transitions between the various muonium states, as outlined in Fig. 2. There are four types of transitions involving different physical processes: ionization (i), thermal activation for simple site changes (a), carrier capture at a specific site (c), and activated capture for combined e^- capture and site-change transitions (ac). The following simple expressions are used to describe these processes: Ionization (activation):

$$\nu_{i(a)} = \rho_{i(a)} \exp[-E_{i(a)}/kT]. \quad (1)$$

Capture:

$$\nu_c = n_e v_e \sigma_c. \quad (2)$$

Activated capture:

$$\nu_{ac} = n_e v_e \kappa_{ac} \exp[-E_{ac}/kT]. \quad (3)$$

ρ , E , σ , and κ are the vibrational prefactor, energy, capture cross section, and composite site-change–electron-capture cross section, respectively, and n_e and v_e are the density and mean thermal velocity for conduction electrons. Similar hole-capture transitions occur in p -type material, but are unimportant in these samples. Integral rate equations describing the evolution of polarization for each center are written and solved using Laplace transform methods for the case where the charged center is on resonance; see the Appendix. The notation we use for specific parameters obtained from fitting to the transition dynamics indicates the initial/

TABLE I. Transitions identified for Mu in silicon along with updated dynamic parameters extracted from rf- μ SR data using the spin-dependent four-state model described in the text. Statistical errors are quoted for energies and capture cross sections.

Mu transition	Rate parameters	
BC charge-state transitions:		
$Mu_{BC}^0 \rightarrow Mu_{BC}^+ + e^-$	$\rho_{BC}^{0/+} = 2.7 \times 10^{13} \text{ s}^{-1}$	$E_{BC}^{0/+} = 0.21 \pm 0.01 \text{ eV}$
$Mu_{BC}^0 + h^+ \rightarrow Mu_{BC}^+$	$\sigma_{BC}^{0/+} = 20 \pm 2 \text{ \AA}^2$	
$Mu_{BC}^+ + e^- \rightarrow Mu_{BC}^0$	$\sigma_{BC}^{+0} = 3300 \pm 300 \text{ \AA}^2$	
T charge-state transitions:		
$Mu_T^0 + e^- \rightarrow Mu_T^-$	$\sigma_T^{0/-} = 8 \pm 2 \text{ \AA}^2$	
$Mu_T^- \rightarrow Mu_T^0 + e^-$	$\rho_T^{-/0} = 2.0 \times 10^{13} \text{ s}^{-1}$	$E_T^{-/0} = 0.56 \pm 0.03 \text{ eV}$
Site-change transitions:		
$Mu_T^0 \rightarrow Mu_{BC}^0$	$\rho_{T/BC}^0 = 4.1 \times 10^{12} \text{ s}^{-1}$	$E_{T/BC}^0 = 0.38 \pm 0.03 \text{ eV}$
Combined charge and site transitions:		
$Mu_{BC}^+ + e^- \rightarrow Mu_T^0$	$\kappa_{BC/T}^{+0} = 2.3 \times 10^{-10} \text{ cm}^2$	$E_{BC/T}^{+0} = 0.40 \pm 0.02 \text{ eV}$
$Mu_{BC}^0 + e^- \rightarrow Mu_T^-$	$\kappa_{BC/T}^{0/-} = 8.4 \times 10^{-9} \text{ cm}^2$	$E_{BC/T}^{0/-} = 0.31 \pm 0.01 \text{ eV}$

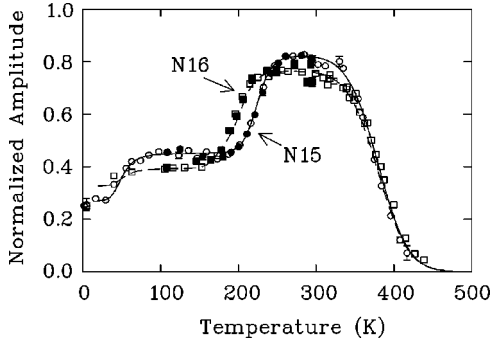
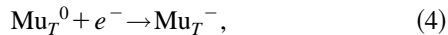


FIG. 3. Normalized rf- μ SR amplitudes for negative muonium in *N15* (circles, solid line), a $\langle 100 \rangle$ sample with a net phosphorus concentration of $1.5 \times 10^{15} \text{ cm}^{-3}$, and *N16* (squares, broken line), a $\langle 111 \rangle$ sample with a donor concentration of $5 \times 10^{15} \text{ cm}^{-3}$. The filled circles and squares are the data with the improved temperature measurement. The old *N15* data from Ref. 6 (open circles) agree with the new *N15* data. A 5-K correction was added to the temperature of the old *N16* data (open squares) to account for the rf heating of the sample, as discussed in Sec. II.

final charge (superscript) and site (subscript) of the transition end states; that is, $E_T^{-/0}$ for the *T*-site ionization energy discussed earlier, or $E_{T/BC}^0$ for the site-change barrier related to the transition from the metastable to stable Mu^0 configuration.

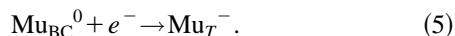
IV. RESULTS AND DISCUSSION

The normalized rf- μ SR amplitudes for diamagnetic muonium as a function of temperature in *N15* (circles) and *N16* (squares) are shown in Fig. 3. We begin discussion of these data with *N15*, a $\langle 100 \rangle$ -oriented sample with a P concentration of $1.5 \times 10^{15} \text{ cm}^{-3}$. Details of the arguments for most transition assignments have been presented previously;⁶ here we present a final assignment, summarize the observed transitions and present updated parameter determinations (see Table I). Starting from the lowest temperature, the initial amplitude is larger than for near-intrinsic samples, and is attributed to ionization of P donors during thermalization of implanted muons and the subsequent capture of two electrons, although no precise information is obtained on these very rapid processes. The next feature with increasing temperature is the rise near 50 K, corresponding to the temperature at which P ionizes thermally. This feature is attributed to electron capture by Mu_T^0 ,



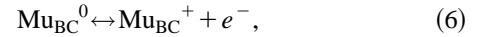
with the temperature dependence controlled by n_e from the donor ionization. Fitting the 50-K step in the *N15* sample yields a cross section of $8 \text{ \AA}^2 (\sigma_T^{0/-})$ for electron capture by Mu_T^0 .

The second feature with increasing temperature, a sharp step near 200 K, is assigned to a combined electron capture and site change leading to Mu_T^- ,



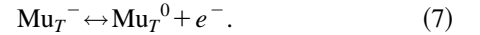
Fitting this step in the *N15* sample to the rate expression in Eq. (3) yields an activation energy for this transition of 0.31 eV ($E_{BC/T}^{0/-}$), and an effective total-process cross section of

$8.4 \times 10^{-9} \text{ cm}^2 (\kappa_{BC/T}^{0/-})$. In modeling this step it is important to include the BC charge-exchange cycle (ionization to Mu_{BC}^+ and electron recapture to Mu_{BC}^0) as discussed earlier, which results in a single step near 200 K when Mu_T^- is formed instead of the double step expected if BC charge exchange did not occur. The parameters used for the BC ionization rate are those obtained from *p*-type samples, where the ionization is not complicated by e^- recapture; an ionization energy of 0.21 eV ($E_{BC}^{0/+}$) and a frequency prefactor of $2.7 \times 10^{13} \text{ s}^{-1} (\rho_{BC}^{0/+})$. These values are slightly different than those given in Ref. 6 due to reexamining the *P11* sample with the improved temperature measurement. The cross section for electron capture at Mu_{BC}^+ obtained in Ref. 6 is inappropriately small for e^- capture by a charged center and the less complicated model failed to adequately reproduce the data from BC ionization in lightly doped *n*-type samples (see, e.g., sample *N12* in Ref. 6). Including the electron-spin-dependent features related to the BC charge cycle in the model significantly improves the fit, and yields a more reasonable capture cross-section of $3300 \text{ \AA}^2 (\sigma_{BC}^{+/0})$ from data on the cyclic processes,



in lightly doped *n*-type samples.¹⁰

Finally, we turn to the primary result from our reinvestigation of *N15* and *N16*. We can now say with considerable confidence that for these samples the drop in the amplitude at high temperature results from thermal ionization of Mu_T^- and the subsequent onset of a *T*-site charge-exchange cycle,



The parameters for the ionization step, an energy of $0.56 \pm 0.03 \text{ eV} (E_T^{-/0})$ and a prefactor of $2 \times 10^{13} \text{ s}^{-1} (\rho_T^{-/0})$, are determined by taking the average of values which best reproduce this feature in each sample independently. Parameters for the capture half of the cycle were determined from the 50-K feature, as discussed earlier, where that transition occurs in isolation.

The two curves in Fig. 3 are calculated using one set of parameters for the transition rates. Additional transitions which are dominant in *p*-type samples were included in modeling the dynamics but had essentially no effect on the shape of these curves. The only difference in calculation of the two curves is that the solid and dashed lines use the P concentration and sample orientation appropriate to the *N15* and *N16* samples, respectively. In comparing the *N15* and *N16* data, the following observations are especially relevant to transition assignments. (1) The shift of the step near 200 K to lower temperature with increased concentration of conduction electrons confirms that this step results from electron capture and the formation of Mu_T^- , consistent with the previous assignment. (2) The high-temperature drop in the amplitude of the diamagnetic signal is independent of the free electron density, confirming that the rate determining step is thermal ionization of Mu_T^- .

For lower electron concentrations a similar feature originates from the Mu_{BC}^+ state, and signals the onset of a more complicated high-temperature charge cycle.⁶ The change in trend for this feature, from a downward temperature shift with increasing n_e observed for lower concentrations to a

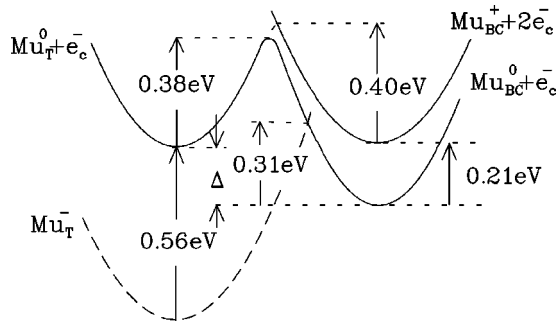


FIG. 4. An idealized configuration-coordinate diagram representing the four states of muonium in silicon. The solid curves represent the states active in p -type samples, and the broken curve is for negative muonium which is required for moderately to heavily doped n -type samples. Experimental values for important energy differences are shown. The energy difference between Mu_T^0 and $\text{Mu}_{\text{BC}}^0(\Delta)$ is plotted as 0.2 eV, but has not been determined experimentally.

higher temperature for $N15$ and $N16$, provided the original clue that its origin was different for these samples. Since Mu_T^- dominates the diamagnetic signal for n_e above the low 10^{14}-cm^{-3} range, the amplitude decrease was assigned to a transition involving Mu_T^- .⁶ The present data allow the transition process to be studied in more detail, and thus provide a determination of the Mu_T^- ionization energy in silicon. An alternative explanation could be that a sharp increase in the rates for competing transitions out of the precursor Mu^0 states rapidly decreases the Mu_T^- formation probability near 350 K. Were this the case, a perceptible shift to higher temperature with increased donor concentration would be observed. Such a feature could also arise from hole capture rather than electron ionization. However, since the temperature is below the extrinsic to intrinsic crossover for these net donor concentrations, the minimum resulting energy parameter would then be the full gap energy which occurs in $n_h(T)$. Each of these alternative explanations is ruled out by the present results.

A schematic configuration-coordinate diagram representing the various muonium states in silicon is shown in Fig. 4. The system includes three particles: the implanted μ^+ and two e^- , either at the bottom of the conduction band or localized at the muonium impurity. The energy differences displayed are scaled to the values we obtain. This is an operational diagram, meaning that the curves represent the lowest energy at each configuration rather than the corresponding potential energy curves. Because of zero-point energy differences and enhanced quantum characteristics in the dynamics of muonium in comparison to hydrogen, the energy parameters in an analogous diagram for H should be slightly different, even within an adiabatic treatment where the two configurational potential energy surfaces would be identical.

Both Figs. 1 and 4 are drawn with the acceptor level deeper than the donor level; however, we do not have conclusive evidence that muonium is a negative- U system in Si since the configuration energy difference Δ must be included in the comparison. Only if Δ is less than 0.35 eV ($E_T^{-/0} - E_{\text{BC}}^{0/+}$) can one conclude that muonium is a negative- U system based on the experimental evidence. Unfortunately, an experimental measurement of the configurational energy

difference between the two Mu^0 states appears to be unobtainable for silicon. Theoretical estimates^{8,11,12} suggest that Δ is a few tenths of an eV, which leaves the question of whether muonium in fact has negative U still unresolved.

V. CONCLUSIONS

Detailed studies of the diamagnetic rf- μ SR amplitude in two moderately to heavily doped n -type Si samples require the presence of Mu_T^- for an explanation. Our analysis establishes that the ionization energy for $\text{Mu}_T^- \rightarrow \text{Mu}_T^0 + e_c^-$ is 0.56 ± 0.03 eV. This places the muonium acceptor level at $0.56 \text{ eV} - \Delta$ below the the conduction-band minimum, where Δ is the energy difference between Mu_T^0 and Mu_{BC}^0 . Since the muonium donor level depth is near 0.2 eV and estimates^{2,8} of Δ are also ~ 0.2 eV, this result suggests that muonium may be a negative- U impurity, but by a considerably smaller margin than the >0.3 eV claimed⁸ for the analogous hydrogen system. Based on the muonium results we would conclude that the rate-limiting step for the series of hydrogen transitions leading from H^- to H^+ is actually $\text{H}_T^- \rightarrow \text{H}_T^0$, and that H_T^0 is most likely metastable even though it has not been directly observed. If this is true, then one of the crucial assumptions⁸ allowing analysis of the hydrogen data based on a detailed balance argument within a subset of the states involved would not be satisfied. The near equivalence of energies associated with ionization of Mu^- and H^- , as well as for energies related to electron-capture transitions from the stable BC configuration of Mu^0 and H^0 into their respective negative charge states, provides strong support for the argument that the energy landscape for isolated Mu and H impurities is essentially identical.

Finally, our data on muonium dynamics show a complicated set of charge-state transitions which are active on a very short time scale compared to measurement times for most hydrogen experiments. These results imply that both the muonium and hydrogen impurity systems in silicon involve a dynamic mix of charge states at ordinary temperatures. As a consequence of such rapid transitions, it may be necessary to reexamine additional assumptions underlying analysis of data on hydrogen defect properties which have commonly relied on the presence of a single state or a simple transition from one state to another.

ACKNOWLEDGMENTS

The authors wish to thank S. K. Estreicher for a critical reading of this manuscript, and numerous discussions of related theoretical results. It is also a pleasure to thank K. H. Chow and C. Schwab for valuable discussion and experimental assistance. This work was supported by grants from the U.S. National Science Foundation [Grant Nos. DMR 96-23611 (T.L.E.) and DMR 96-23823 (R.L.L.)], and the Robert A. Welch Foundation [Grant No. D-1321 (R.L.L.)].

APPENDIX: FOUR-STATE MODEL

The following muonium states are observed in Si: Mu_{BC}^+ , Mu_T^- , Mu_{BC}^0 , and Mu_T^0 . In addition, for neutral muonium the spin of the unpaired electron can point up (i.e., parallel to the external field) or down. Many transitions be-

tween these states have been identified and are shown in Fig. 2. As discussed in Sec. III, very simple temperature-dependent expressions are used for the transition rates.

It was observed in Ref. 6 that there is no diamagnetic amplitude at low temperature in the near-intrinsic sample, and that this amplitude increases for doped samples. In the four-state model discussed here we assume that all the polarization at low temperature ($T=0$) is in the two neutral prompt states $\text{Mu}_{\text{BC}}^0(P_{0,z}^{\text{Mu}_{\text{BC}}^0})$ and $\text{Mu}_T^0(P_{0,z}^{\text{Mu}_T^0})$. The increase in the low-temperature diamagnetic amplitude in the doped samples is attributed to the ionization of P donors during thermalization of implanted muons and the subse-

quent capture of electrons.⁶ This increase is accompanied by a decrease in the initial Mu_T^0 amplitude and is described in the four-state model by adding a term proportional to the concentration of P donors to the $\nu_T^{0/-}$ capture rate. However, since no precise information is obtained on these very rapid processes, they will not be discussed further in this work.

Only the \hat{z} component of the polarization is detected in a rf μ SR experiment. Employing a strong collision model, the following integral rate equations describe the time evolution of the muon spin polarization for the various muonium states:

$$\begin{aligned} P_z^{\text{Mu}_{\text{BC}}^{0\uparrow}}(t) = & \frac{1}{2} P_{0,z}^{\text{Mu}_{\text{BC}}^0} G_z^{\text{Mu}_{\text{BC}}^{0\uparrow}}(t) e^{-(\nu_{\text{BC}}^{0/+} + \nu_{\text{BC}/T}^{0/-})t} \\ & + \nu_{T/\text{BC}}^0 \int_0^t P_z^{\text{Mu}_T^{0\uparrow}}(\tau) G_z^{\text{Mu}_{\text{BC}}^{0\uparrow}}(t-\tau) e^{-(\nu_{\text{BC}}^{0/+} + \nu_{\text{BC}/T}^{0/-})(t-\tau)} d\tau \\ & + \frac{1}{2} \nu_{\text{BC}}^{+/0} \int_0^t P_z^{\text{Mu}_{\text{BC}}^+}(\tau) G_z^{\text{Mu}_{\text{BC}}^{0\uparrow}}(t-\tau) e^{-(\nu_{\text{BC}}^{0/+} + \nu_{\text{BC}/T}^{0/-})(t-\tau)} d\tau. \end{aligned} \quad (\text{A1})$$

The muon's polarization while in the $\text{Mu}_{\text{BC}}^{0\uparrow}$ state is given by (see Appendix B of Ref. 6):

$$G_z^{\text{Mu}_{\text{BC}}^{0\uparrow}}(t) = \sum_j f_j [\cos^2 \vartheta_\mu^{\uparrow j} + \sin^2 \vartheta_\mu^{\uparrow j} \cos \omega_\mu^{\uparrow j} t], \quad (\text{A2})$$

where f_j is the occupation fraction, $|\omega_\mu^{\uparrow j}|$ is the strength, and $\vartheta_\mu^{\uparrow j}$ is the polar angle of the effective field from the up muonium electron. Similar equations can be written to describe the time evolution of the polarization for $\text{Mu}_{\text{BC}}^{0\downarrow}[P_z^{\text{Mu}_{\text{BC}}^{0\downarrow}}(t)]$.

The time evolution of the polarization for $\text{Mu}_T^{0\uparrow}$ is given by

$$\begin{aligned} P_z^{\text{Mu}_T^{0\uparrow}}(t) = & \frac{1}{2} P_{0,z}^{\text{Mu}_T^0} G_z^{\text{Mu}_T^{0\uparrow}}(t) e^{-(\nu_{T/\text{BC}}^0 + \nu_T^{0/-})t} \\ & + \frac{1}{2} \nu_{\text{BC}/T}^{+/0} \int_0^t P_z^{\text{Mu}_{\text{BC}}^+}(\tau) G_z^{\text{Mu}_T^{0\uparrow}}(t-\tau) e^{-(\nu_{T/\text{BC}}^0 + \nu_T^{0/-})(t-\tau)} d\tau \\ & + \frac{1}{2} \nu_T^{-/0} \int_0^t P_z^{\text{Mu}_T^-}(\tau) G_z^{\text{Mu}_T^{0\uparrow}}(t-\tau) e^{-(\nu_{T/\text{BC}}^0 + \nu_T^{0/-})(t-\tau)} d\tau, \end{aligned} \quad (\text{A3})$$

where the muon's polarization while in $\text{Mu}_T^{0\uparrow}$ is given by¹³

$$G_z^{\text{Mu}_T^{0\uparrow}}(t) = (1 - a_{24}) + a_{24} \cos \omega_{24} t, \quad (\text{A4})$$

with a_{24} the muonium precession amplitude and ω_{24} the precession frequency for the 2-4 transition. For isotropic neutral muonium Mu_T^0 , the polarization $P_z^{\text{Mu}_T^{0\downarrow}}(t) = P_z^{\text{Mu}_T^{0\uparrow}}(t)$.

The time evolution of the polarization of the two diamagnetic states are given by

$$P_z^{\text{Mu}_{\text{BC}}^+}(t) = \nu_{\text{BC}}^{0/+} \int_0^t [P_z^{\text{Mu}_{\text{BC}}^{0\uparrow}}(\tau) + P_z^{\text{Mu}_{\text{BC}}^{0\downarrow}}(\tau)] G_z^{\text{Mu}_{\text{BC}}^+}(t-\tau) e^{-(\nu_{\text{BC}}^{+/0} + \nu_{\text{BC}/T}^{+/0})(t-\tau)} d\tau \quad (\text{A5})$$

and

$$\begin{aligned} P_z^{\text{Mu}_T^-}(t) = & \nu_{\text{BC}/T}^{0/-} \int_0^t [P_z^{\text{Mu}_{\text{BC}}^{0\uparrow}}(\tau) + P_z^{\text{Mu}_{\text{BC}}^{0\downarrow}}(\tau)] G_z^{\text{Mu}_T^-}(t-\tau) e^{-\nu_T^{-/0}(t-\tau)} d\tau \\ & + \nu_T^{0/-} \int_0^t [P_z^{\text{Mu}_T^{0\uparrow}}(\tau) + P_z^{\text{Mu}_T^{0\downarrow}}(\tau)] G_z^{\text{Mu}_T^-}(t-\tau) e^{-\nu_T^{-/0}(t-\tau)} d\tau, \end{aligned} \quad (\text{A6})$$

where $G_z^{\text{MuBC}^+}(t)$ and $G_z^{\text{MuT}^-}(t)$ are the time evolution of the polarization while in the MuBC^+ and MuT^- states, respectively. For both cases the time evolution is equal to $\cos(\omega_1 t)$ on resonance and unity far off resonance.

The Laplace transforms of the polarization are

$$\bar{P}_z^{\text{MuBC}^0}(s) = \frac{\bar{G}_z^{\text{MuBC}^0} \left[\frac{1}{2} P_{0,z}^{\text{MuBC}^0} + \nu_{T/BC}^0 \bar{C} P_{0,z}^{\text{MuT}^0} \right]}{1 - \bar{G}_z^{\text{MuBC}^0} \bar{D}}, \quad (\text{A7})$$

$$\bar{G}_z^{\text{MuBC}^0} = \bar{G}_z^{\text{MuBC}^{0\uparrow}} (s + \nu_{BC}^{0/+} + \nu_{BC/T}^{0/-}) + \bar{G}_z^{\text{MuBC}^{0\downarrow}} (s + \nu_{BC}^{0/+} + \nu_{BC/T}^{0/-}), \quad (\text{A8})$$

$$\bar{C} = \frac{\frac{1}{2} \bar{G}_z^{\text{MuT}^{0\uparrow}} (s + \nu_{T/BC}^0 + \nu_T^{0/-})}{1 - \nu_T^{-/0} \nu_T^{0/-} \bar{G}_z^{\text{MuT}^-} (s + \nu_T^{-/0}) \bar{G}_z^{\text{MuT}^{0\uparrow}} (s + \nu_{T/BC}^0 + \nu_T^{0/-})}, \quad (\text{A9})$$

$$\bar{D} = (\nu_{T/BC}^0 \nu_{BC/T}^{+/0} \bar{C} + \frac{1}{2} \nu_{BC}^{+/0}) \nu_{BC}^{0/+} \bar{G}_z^{\text{MuBC}^+} (s + \nu_{BC}^{+/0} + \nu_{BC/T}^{+/0}) + \nu_{T/BC}^0 \nu_T^{-/0} \nu_{BC/T}^{0/-} \bar{C} \bar{G}_z^{\text{MuT}^-} (s + \nu_T^{-/0}), \quad (\text{A10})$$

$$\bar{P}_z^{\text{MuBC}^+}(s) = \nu_{BC}^{0/+} \bar{G}_z^{\text{MuBC}^+} (s + \nu_{BC}^{+/0} + \nu_{BC/T}^{+/0}) \bar{P}_z^{\text{MuBC}^0}(s), \quad (\text{A11})$$

$$\bar{P}_z^{\text{MuT}^0}(s) = 2\bar{C} [P_{0,z}^{\text{MuT}^0} + \nu_{BC/T}^{+/0} \bar{P}_z^{\text{MuBC}^+}(s) + \nu_T^{-/0} \nu_{BC/T}^{0/-} \bar{G}_z^{\text{MuT}^-} (s + \nu_T^{-/0}) \bar{P}_z^{\text{MuBC}^0}(s)], \quad (\text{A12})$$

$$\bar{P}_z^{\text{MuT}^-}(s) = \bar{G}_z^{\text{MuT}^-} (s + \nu_T^{-/0}) [\nu_{BC/T}^{0/-} \bar{P}_z^{\text{MuBC}^0}(s) + \nu_T^{0/-} \bar{P}_z^{\text{MuT}^0}(s)], \quad (\text{A13})$$

$$\bar{P}_z^{\text{dia}}(s) = \bar{P}_z^{\text{MuBC}^+}(s) + \bar{P}_z^{\text{MuT}^-}(s). \quad (\text{A14})$$

The rf-induced asymmetry of the diamagnetic centers ($A_{\text{rf}}^{\text{dia}}$), which is the measured quantity experimentally, is given by⁶

$$A_{\text{rf}}^{\text{dia}} = \nu_{\mu} [\bar{P}_z^{\text{dia,off}}(\nu_{\mu}) - \bar{P}_z^{\text{dia,on}}(\nu_{\mu})], \quad (\text{A15})$$

where ν_{μ} is the inverse muon lifetime, and $\bar{P}_z^{\text{dia,off}}$ and $\bar{P}_z^{\text{dia,on}}$ are the Laplace transforms of the diamagnetic polarization with the rf off ($\omega_1=0$) and rf on, respectively. This asymmetry contains the polarization history from all precursor states and transitions introduced in this model.

¹S. M. Myers, M. I. Baskes, H. M. Birnbaum, J. W. Corbett, G. G. DeLeo, S. K. Estreicher, E. E. Haller, P. Jena, N. M. Johnson, R. Kirchheim, S. J. Pearton, and M. J. Stavola, *Rev. Mod. Phys.* **64**, 559 (1992).

²S. K. Estreicher, *Mater. Sci. Eng.* **R14**, 319 (1995).

³R. F. Kiefl and T. L. Estle, in *Hydrogen in Semiconductors*, edited by J. I. Pankove and N. M. Johnson, *Semiconductors and Semimetals*, Vol. 34 (Academic, New York, 1990), p. 547.

⁴K. H. Chow, B. Hitti and R. F. Kiefl, in *μ SR on Muonium in Semiconductors and Its Relation to Hydrogen*, edited by M. J. Stavola, *Semiconductors and Semimetals*, Vol. 51 (Academic, New York 1998), p. 137.

⁵H. Simmler, P. Eschle, H. Keller, W. Kündig, W. Odermatt, B. D. Patterson, B. Pümpin, I. M. Savić, J. W. Schneider, U. Straumann, and P. Trüöl, *Hyperfine Interact.* **64**, 535 (1990).

⁶S. R. Kreitzman, B. Hitti, R. L. Lichti, T. L. Estle, and K. H. Chow, *Phys. Rev. B* **51**, 13 117 (1995).

⁷K. H. Chow, R. L. Lichti, R. F. Kiefl, S. Dunsiger, T. L. Estle, B. Hitti, R. Kadono, W. A. MacFarlane, J. W. Schneider, D. Schumann, and M. Shelley, *Phys. Rev. B* **50**, 8918 (1994).

⁸N. M. Johnson, C. Herring, and C. Van de Walle, *Phys. Rev. Lett.* **73**, 130 (1994). See also Comment and Reply: C. H. Seager, R. A. Anderson, and S. K. Estreicher, *ibid.* **74**, 4565 (1995); N. M. Johnson, C. Herring, and C. Van de Walle, *ibid.* **74**, 4566 (1995).

⁹J. S. Blakemore, *Semiconductor Statistics* (Dover, New York, 1987), p. 117.

¹⁰B. Hitti, S. R. Kreitzman, T. L. Estle, R. L. Lichti, and E. C. Lightowers, *Hyperfine Interact.* **105**, 321 (1997).

¹¹C. G. Van de Walle, P. J. H. Denteneer, Y. Bar-Yam, and S. T. Pantelides, *Phys. Rev. B* **39**, 10 791 (1989).

¹²C. H. Chu and S. K. Estreicher, *Phys. Rev. B* **42**, 9486 (1990).

¹³B. D. Patterson, *Rev. Mod. Phys.* **60**, 69 (1988).